PROCEEDINGS OF SPIE

SPIEDigitalLibrary.org/conference-proceedings-of-spie

Novel vacuum packaged 384 x 288 broadband bolometer FPA with enhanced absorption in the 3-14 µm wavelength range

Bruno Fisette, Mathieu Tremblay, Hassane Oulachgar, Francis Généreux, David Béland, et al.

Bruno Fisette, Mathieu Tremblay, Hassane Oulachgar, Francis Généreux, David Béland, Patrick Beaupré, Christian Julien, David Gay, Sébastien Deshaies, Marc Terroux, Bruno Tremblay, Denis Dufour, Christine Alain, "Novel vacuum packaged 384 x 288 broadband bolometer FPA with enhanced absorption in the 3-14 µm wavelength range," Proc. SPIE 10177, Infrared Technology and Applications XLIII, 101771R (3 May 2017); doi: 10.1117/12.2255747

SPIE.

Event: SPIE Defense + Security, 2017, Anaheim, California, United States

Novel vacuum packaged 384 x 288 broadband bolometer FPA with enhanced absorption in the 3-14 μm wavelength range

Bruno Fisette*, Mathieu Tremblay, Hassane Oulachgar, Francis Généreux, David Béland, Patrick Beaupré, Christian Julien, David Gay, Sébastien Deshaies, Marc Terroux, Bruno Tremblay, Denis Dufour and Christine Alain
INO, 2740 Einstein Street, Quebec, Quebec, Canada, G2P 4S4

ABSTRACT

This paper reports on the development of a fully packaged focal plane array of broadband microbolometers. The detector makes use of a gold black thin film to expand its absorption range from 3 to 14 μm. A low temperature packaging process was developed to minimize sintering of the gold black absorber during vacuum sealing of the bolometer array package. The gold black absorber was also laser trimmed to prevent lateral diffusion of heat and promote a better MTF. The resulting FPAs show a NETD lower than 25 mK at a frame rate of 50 Hz.

Keywords: Infrared, Uncooled, Microbolometer, 35 μm, Gold black, Packaging, Focal Plane Array

1. INTRODUCTION

INO has been active in the development of customized uncooled bolometers for more than 20 years[1-6]. Microbolometers are used in several fields, including space applications for Earth observation[3-5] and airborne applications for far infrared sensing of thin ice clouds[7-9]. As uncooled microbolometer requires a pressure below 10 mTorr to work efficiently[10], INO has also been active in vacuum sealed packaging for more than 20 years[2,11-13]. INO has especially been involved in the development of packaging of bolometer FPAs for space applications, like the New Infared Sensor Technology (NIRST) instrument, one of the payloads of the SAC-D/Aquarius satellite launched in 2011, for which INO supplied the IR camera module[14].

The capacity to deposit gold black thin films on top of bolometer pixel array has enabled the development of highly sensitive FPA with nearly flat spectral response[15]. Until now, most of the applications have been limited to flight instruments where vacuum sealed packaging is not required[16-17]. However, several terrestrial applications such as spectral imaging may benefit from a vacuum sealed uncooled FPA with a flat spectral response. The main hindrance in realizing a vacuum seal of the blacked FPA is the sintering of gold black thin films upon prolonged exposure to elevated temperature[18]. Since elevated temperature exposure is required for several steps of standard packaging processes, especially for outgassing purposes, the vacuum packaging of gold black coated detectors has long been considered as unpractical.

INO has developed a high-reliability and scalable packaging platform for space applications[13]. For the TICFIRE mission, a gold black coated FPA must be added to the detector package. A low temperature packaging process was thereby developed to vacuum seal the gold backed FPA[9]. This low temperature packaging process was adapted and a more compact package was conceived to extend this technology to terrestrial applications. A new bolometer architecture especially conceived to receive a gold black coating was also developed.

In this paper, the performance of this new FPA is compared to INO's standard FPAs in terms of NEP, NETD and response time. The specific detectivity, D*, of the bolometers in the 3 to 14 μm wavelength band is presented. The main characteristics of the package are also discussed in details.

*Bruno.Fisette@ino.ca; phone 1 418 657-7006; fax 1 418 657-7009; www.ino.ca

Infrared Technology and Applications XLIII, edited by Bjørn F. Andresen, Gabor F. Fulop, Charles M. Hanson, John L. Miller, Paul R. Norton, Proc. of SPIE Vol. 10177, 101771R · © 2017 SPIE
CCC code: 0277-786X/17/$18 · doi: 10.1117/12.2255747

2. DESIGN AND FABRICATION OF THE PACKAGE

2.1 Microbolometer

INO's uncooled 384 x 288 microbolometer focal plane array (FPA) with a 35 µm pitch was used as a platform to demonstrate the efficiency of the package design and assembly process. The microbolometer was fabricated on CMOS integrated readout circuits using surface micromachining techniques. INO's microbolometer FPA is based on vanadium oxide technology. The typical temperature coefficient of resistance of a vanadium oxide thermistor is below 2.1 %/K. The microbolometer pixels were constructed using PECVD silicon nitride thin film as a structural material and spin coated polyimide as a sacrificial layer. This 35 microns pitch uncooled microbolometer focal plane array was described in a previous paper[19].

To enhance the spectral absorption of uncooled microbolometer pixel arrays, the FPAs were coated with a relatively thick 25 to 40 µm gold black thin film deposited using an evaporation process performed at INO. Spectroscopic measurements obtained for various deposition conditions and film thicknesses showed that the specular reflectance of the gold black coating is less than 10 % in the wavelength range from 0.2 to 100 µm which makes it an excellent broadband absorber for both infrared and terahertz radiation[15]. The typical gold black specular reflectance as function of wavelength is presented in Figure 1.

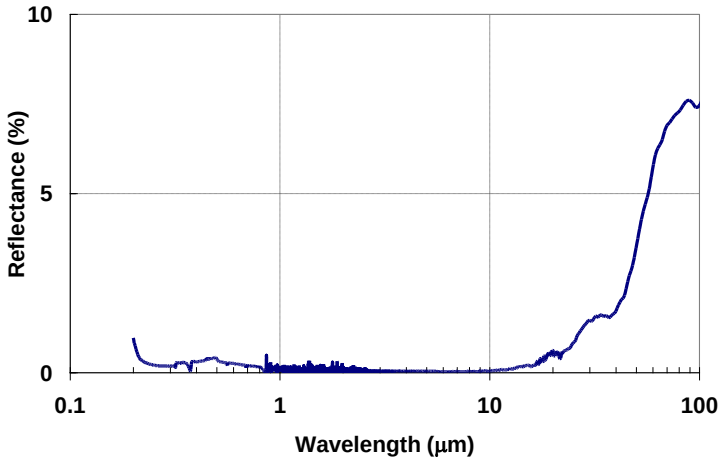

Figure 1. Specular reflectance of a 31 µm gold black film measured between 0.2 µm and 100 µm.

2.2 Laser trimming of gold black

The gold black layer inherently creates thermal short between the bolometer pixels. To singulate and preserve the electrical and thermal isolation of each pixel[15,23], narrow trenches are made in the gold black layer using a laser trimming process developed at INO. To laser trim an entire matrix of 384 x 288 pixels, a new high speed laser station with micrometric accuracy was assembled. Trench widths of ≤ 4 µm are processed in gold black layers with thicknesses ranging from 25 µm to 40 µm by using picosecond pulses (Δt = 35 ps) at 532 nm with a high beam quality ($M^2 < 1.2$), thus preserving a significant fill factor. The laser pulses are emitted from a fiber laser source in a Master Oscillator – Power Amplification architecture developed at INO (MOPAW) that emits 25 W of IR power at repetition rates ranging from single shot to 1 MHz. The laser includes a sophisticated modulated seed system that generates arbitrarily shaped pulse envelopes with durations varying from 2.5 ns to 500 ns and containing one or multiple ps or ns pulses[24]. Precision motorized XY-Theta stages coupled to a high-resolution vision system allow positioning of the microbolometer FPA with an accuracy better than 1 µm with respect to the focused laser spot. Figure 2 shows a section of a 384 x 288 gold black coated FPA that has been laser trimmed between the pixels using picosecond pulses.

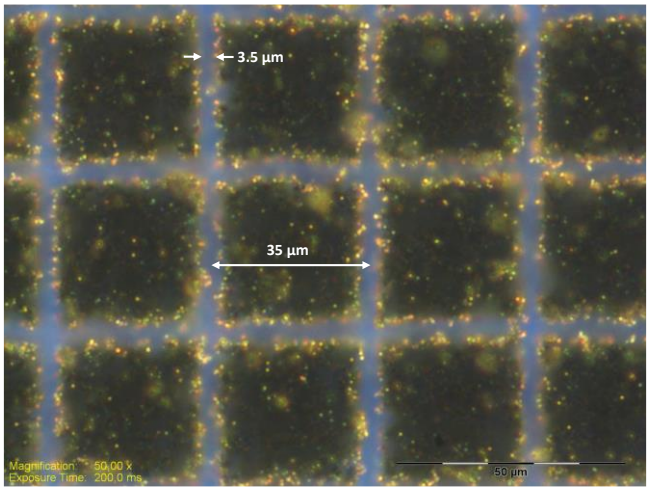

Figure 2. Section of a 384 x 288 FPA covered with a 30 µm-thick gold black layer laser trimmed using INO's MOPAW laser.

2.3 Package design

INO has previously reported on the development of a packaging platform for large FPAs in high-reliability applications[13] and has adapted it to a low temperature process for a gold blacked die[9]. The package must accommodate a gold blacked 384 x 288 microbolometer FPA and its size must be minimized to be compatible with INO's MicroXcam camera electronics[20]. By design, the package must meet MIL-STD-810 specifications for temperature, mechanical shocks and random vibrations, as listed in Table 1.

Table 1. MIL-STD-810 requirements for package

Test	Method	Parameters
Thermal cycling	501 502	7 cycles from 25°C to +60°C 1 cycle from 25°C to -40°C
Random vibrations	514	Cargo Plane (4.02 Grms in amplitude on all axes) Truck Transportation (1.04 Grms in amplitude on all axes)
Mechanical shocks	516	Transit Drop from 122 cm, 26 drops

Figure 3 presents the design of this package. The base contains a slot and a pin hole to align the package with regard to the optical axis of the imaging lens. Four other mounting holes are used to attach it to the imaging system. The Kovar base is plated with Au on Ni to avoid corrosion. An oxygen-free copper pumping tube is added to the package base. This tube is used to create a vacuum inside the cavity by pumping through it and then pinching it hermetically.

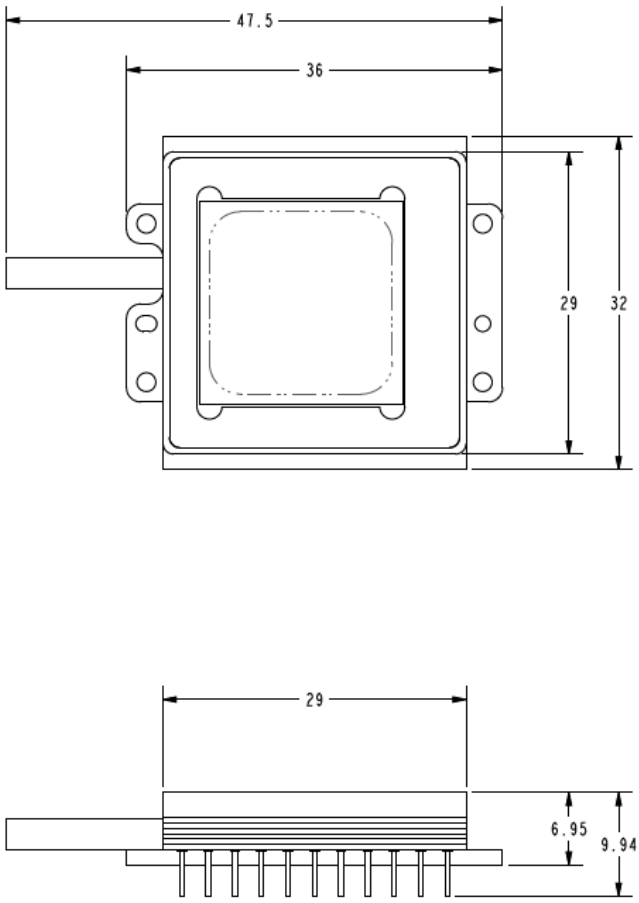

Figure 3. Metallic package with ceramic inserts design, dimensions are in millimeters

The key components of the package are the high temperature cofired ceramic inserts, allowing to hermetically seal the electrical feedthroughs. These feedthroughs consist of external pins brazed on the external surface to prevent leaks along the pins. They are connected to internal pads through multilayer metallic routing between ceramic layers. The two ceramic inserts are co-registred for connection on the same electronic board. A space is reserved on one of the ceramic insert to connect an INO MEMS-pirani gauge[21] which monitors the pressure inside the package with an accuracy of ≥ 1 mTorr. In total, the package contains 44 electrical pins.

A high-temperature thermoelectric cooler (TEC) controls the detector temperature as monitored by a thermistor. The TEC has a surface area of 16 X 16 mm^2, which accommodates both the FPA and the thermistor. The package also contains a re-fireable getter introduced to extend lifetime. This getter can be electrically activated by injection of an electrical current, which heats the getter. As the activation temperature of the getter could be higher than the detector or other components maximum allowable temperatures, a radiation shield is added between the getter and the TEC. Figure 4 shows the base assembly of the package with several components fixed and wirebonded. As few as possible volatile components are used in the package assembly to minimize outgassing.

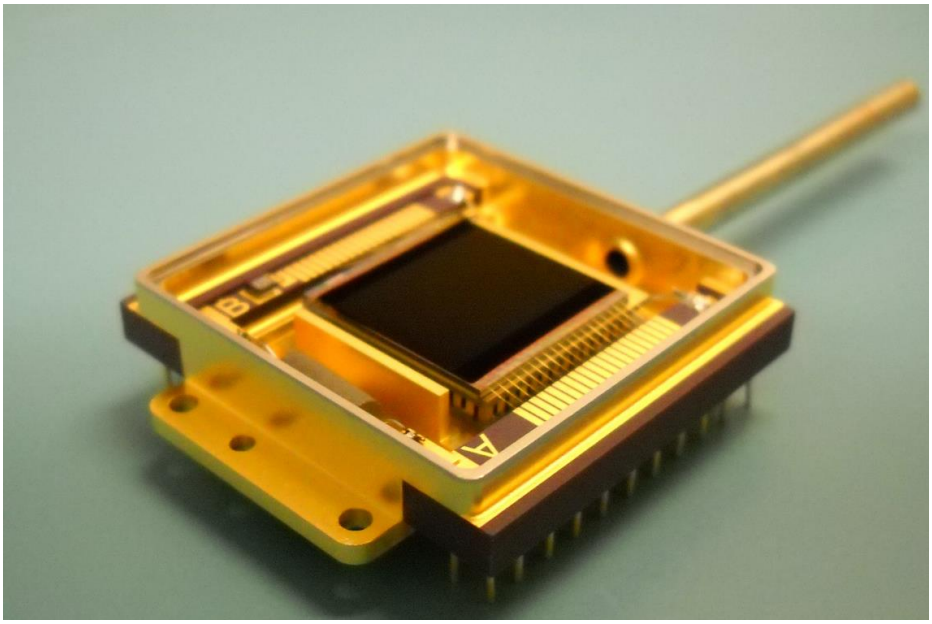

Figure 4. Package base assembly, including a gold blacked FPA.

The cover of the package is made of Kovar and is Ni-plated to avoid corrosion with a Au coating in the window attachment area. The window is made of germanium with a 3 to 14 μm broadband AR coating. The window dimensions were optimized for an F-number of 0.7. Also, the distance between the FPA and the window was minimized to ensure a large field of view.

Optomechanical simulations were performed with ANSYS to optimize the package geometry, soldering material and adhesive. The mesh model is presented in figure 5. This model was used to verify the impact of the temperature, vibrations and stresses on the package. For example, the thickness of the Kovar base was optimized to maximize the heat transfer while ensuring good flatness at the bottom of the package base.

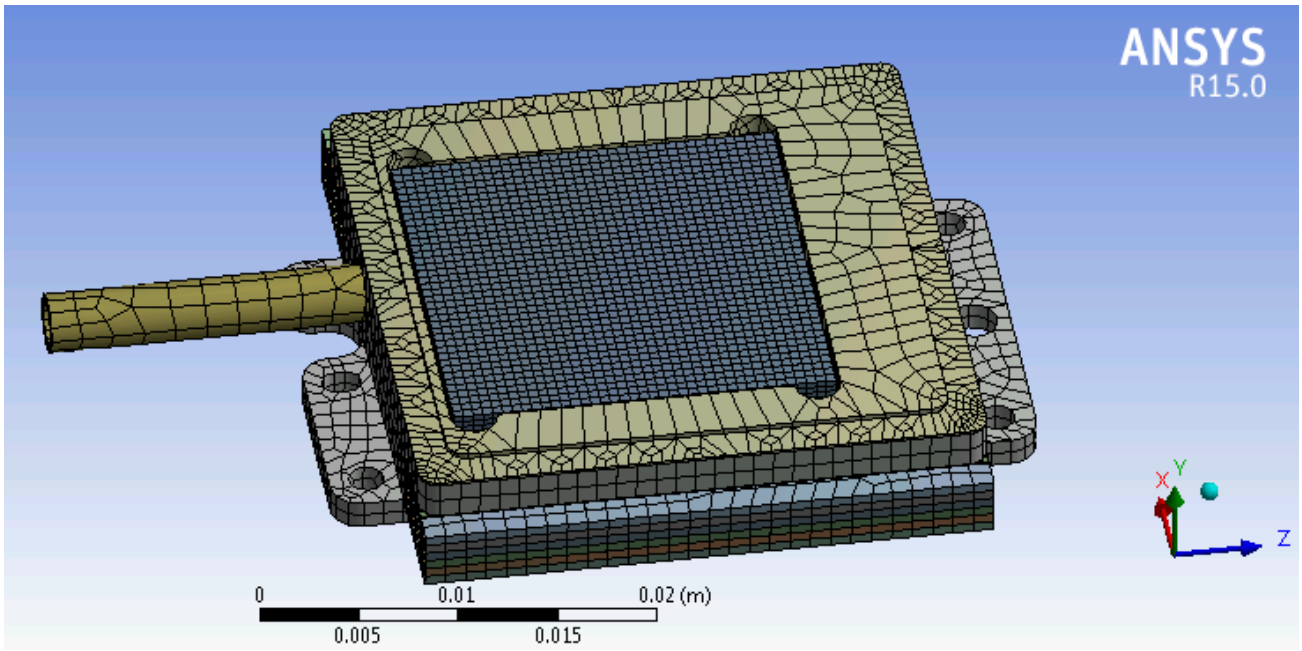

Figure 5. Finite element model used to optimize the package geometry, soldering material and adhesive

2.4 Packaging process

Reflectance measurements on gold black samples heated under vacuum to 70°C during 7 days indicate no significant change for wavelengths from 3 to 14 µm. These results are presented on Figure 6. The packaging process was developed accordingly. The base and the cover are assembled separately. For the base, low temperature processes are required to prevent damage to the gold black layer on the top of the FPA. Thereafter, the base and the cover are hermetically joined. The hermetic joining process is relatively fast to perform and the thermal mass of the package assembly is sufficient to keep the temperature below 45°C, as read live from the package thermistor during the process.

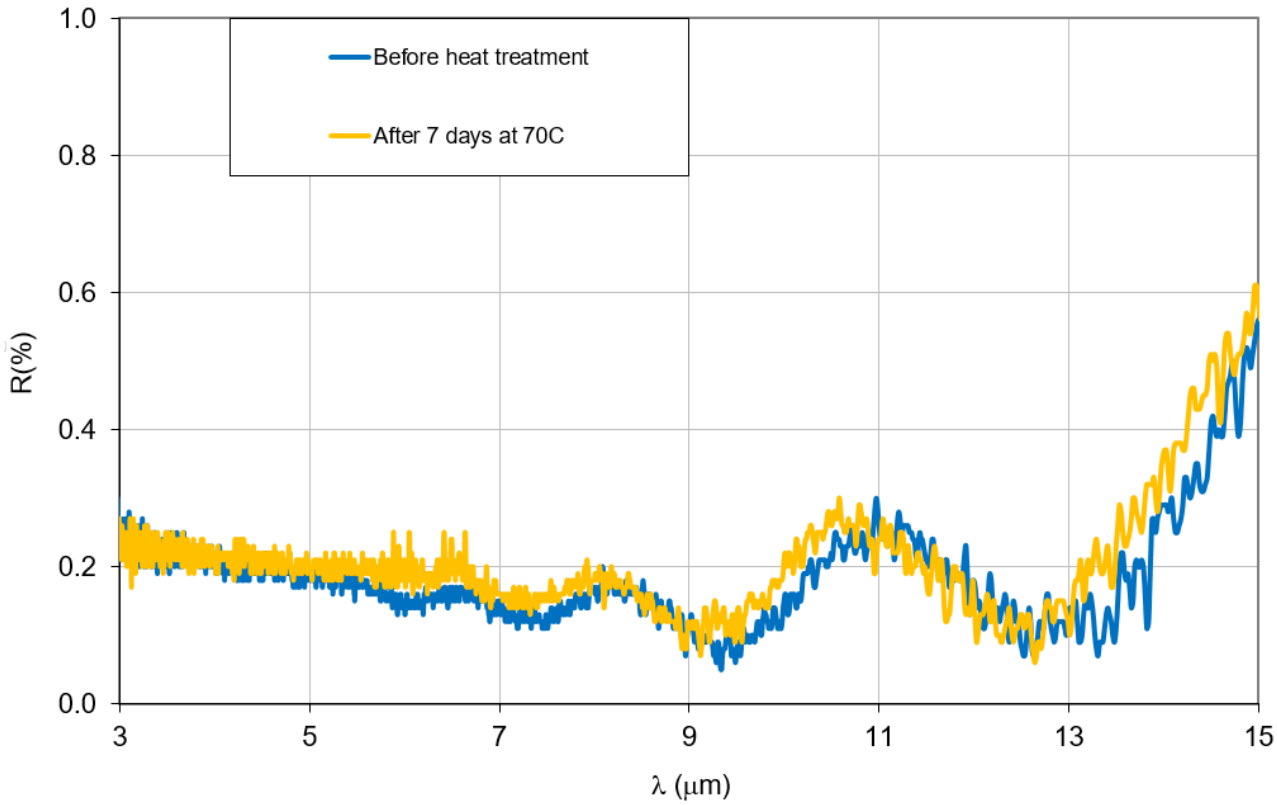

Figure 6. Gold black reflectance before and after 7 days bakeout at 70°C

Thereafter, the package is installed on INO's pumping and pinching station[13] for vacuum bakeout. The vacuum bakeout process was however adapted to be run for a longer time period at a lower temperature than standard. The conductivity of the vacuum through a tube is related to its diameter and length, and is proportional to the square root of the process temperature[22]. To compensate for a lower temperature, and consequently for a lower vacuum conductivity through the pinching tube, the pumping time was increased with regards to our standard pumping process for the same geometry of pinching tube. The thermistor inside the package can be read to ensure the temperature inside the package does not exceed the gold black limits. After pumping, the hydraulic pinching tool is positioned to pinch the copper tube. The base pressure of the package is given by measurement with the MEMS-pirani sensor inside the package after tube pinching. The getter activation is then performed. The setup is controlled by a computer that monitors the thermistor inside the package to avoid high temperature increases on the FPA during current injection. Figure 7 shows the package after completion of assembly and vacuum sealing.

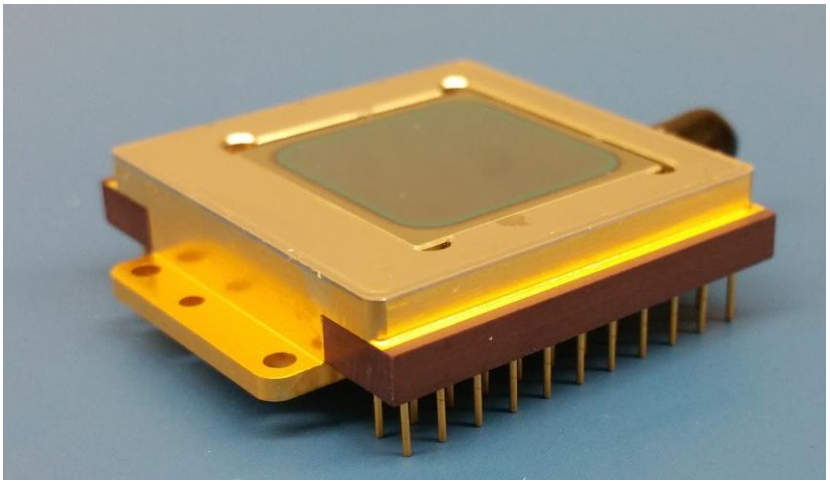

Figure 7. Vacuum-sealed package

3. PERFORMANCE OF THE LOW TEMPERATURE PACKAGING PROCESS

In this section, the methodology for the characterization of the packages sealed using the low temperature packaging process is described. The first main characteristic is the comparison between the FPA performances reached in dynamic vacuum pumping before vacuum sealing and the performances obtained with the same packaged FPA after vacuum sealing. The second main characteristic is the evolution of the pressure inside the sealed package with time.

3.1 Base pressure

Figure 8 presents the NETD measured on the FPA of one package in dynamic pumping before vacuum sealing of the package. The NETD significantly increases for pressure levels higher than 10 mTorr. This is consistent with the behavior usually observed for VOx-bolometers in other packages[10,25]. Also, this Figure shows the best NETD this specific bolometer FPA is able to reach. It will be the baseline for measurement after pinching of the copper tube.

The methodology for the measurement of the MEMS-pirani sensor was presented in details in a previous paper[26]. The MEMS-pirani sensor indicates a pressure < 1 mTorr after vacuum sealing, while the NETD is 1.07 times the baseline set during dynamic pumping. Therefore, a good vacuum level can be obtained using a low temperature pumping and pinching process presented herein.

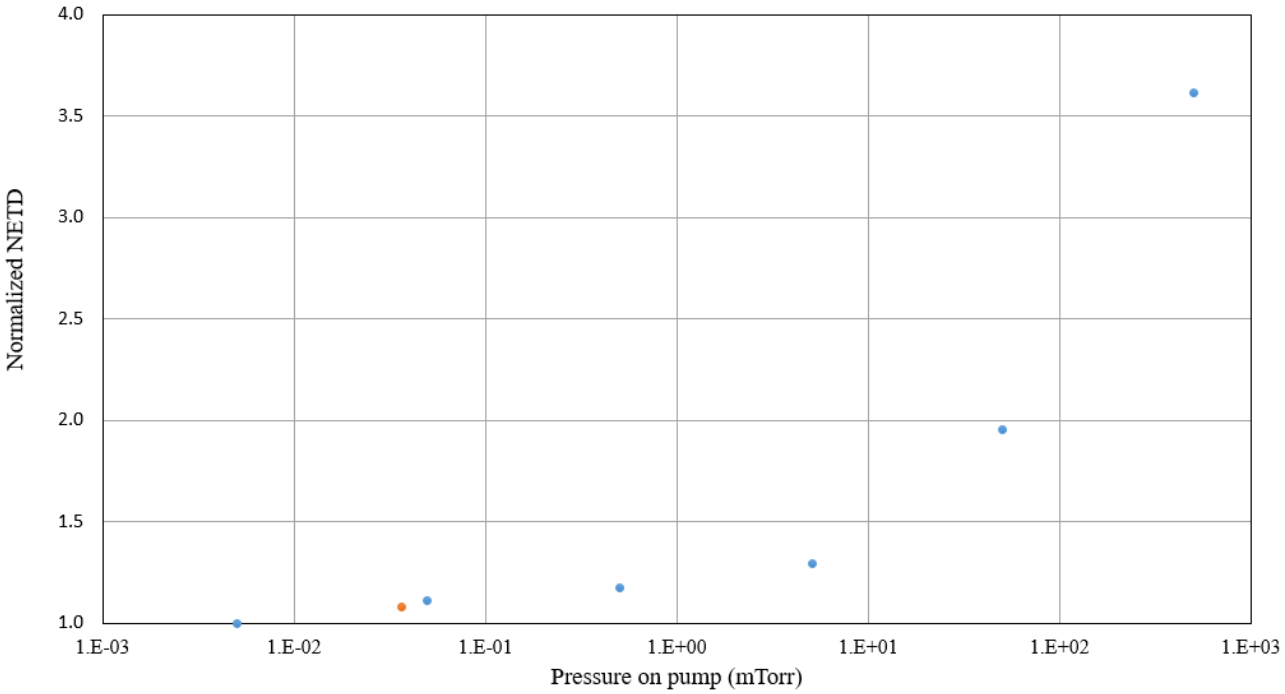

Figure 8. Normalized NETD in dynamic pumping mode (in blue) and after vacuum sealing (in orange)

3.2 Evolution of the pressure in time

The MEMS-pirani sensor of a given package was monitored during several months after vacuum sealing. Generally, the outgassing is more important in a vacuum package during the first days after the pinching of the tube. The pressure was measured to remain below the measurement threshold of the pressure gauge over more than 204 days after vacuum sealing, i.e. $\leq$ 1 mTorr. The absence of cavity pressure change proves the hermeticity of the package and the low outgassing inside the cavity.

4. PERFORMANCE OF THE VACUUM PACKAGED BROADBAND FPA

In this section, the methodologies used for the characterization of the different performance parameters for the vacuum packaged broadband 384 x 288 microbolometer FPA are described. The performances are presented in terms of NETD, NEP, detectivity and response time. Measurements were performed under dynamic vacuum pumping prior to vacuum sealing of the packages. A dynamic pumping approach was favored to remove the contribution of the package base pressure on the performance. All of the following tests were performed on two different 384 x 288 bolometers FPA packaged using the same process. The first FPA is a standard INO's 384 x 288 without gold black. The second FPA is the updated INO 384 x 288 FPA with gold black.

4.1 NETD results

The methodology used to measure the NETD in the packages has been described in a previous paper[10]. In this work, the NETD was characterized for scene temperatures ranging between 20°C and 40°C. The following measurement parameters were used: broadband AR-coated Ge window (3 to 14 µm wavelength), integration time = 40µs, F-number = F/1, TEC temperature = 25°C and frame rate = 50 Hz. The estimated error on NETD measurement is 5%.

The NETD of the standard INO 384 x 288 FPA without gold black is 60 mK. This value is consistent with past results[27]. The updated INO 384 x 288 FPA with gold black shows a lower NETD at 22 mK. Figure 9 presents the NETD histogram of the gold blacked FPA.

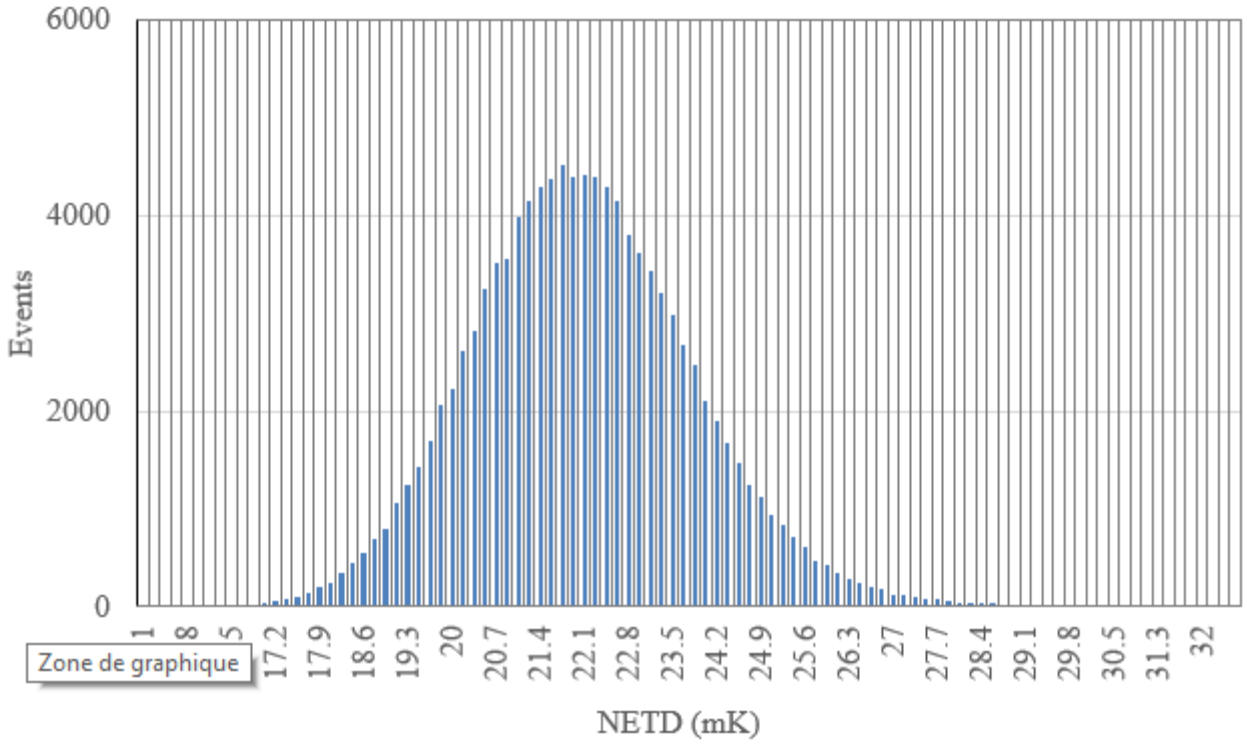

Figure 9. Measured NETD distribution of INO's 384 x 288 FPA with gold black.

4.2 NEP results

The methodology used to measure the NEP in the packages has been described in a previous paper[13]. In this work, the same device parameters are used for both NETD and NEP measurements.

The NEP of the standard INO 384 x 288 FPA is 72 pW. The updated INO 384 x 288 FPA with gold black shows a lower NEP value of 26 pW.

Figure 10 illustrates the relative NEP as function of the wavelength. As shown on this plot, the NEP for the updated INO 384 x 288 FPA with gold black is not only lower, it is also more uniform over the entire spectral band, thanks to the flat absorption of the gold black thin film.

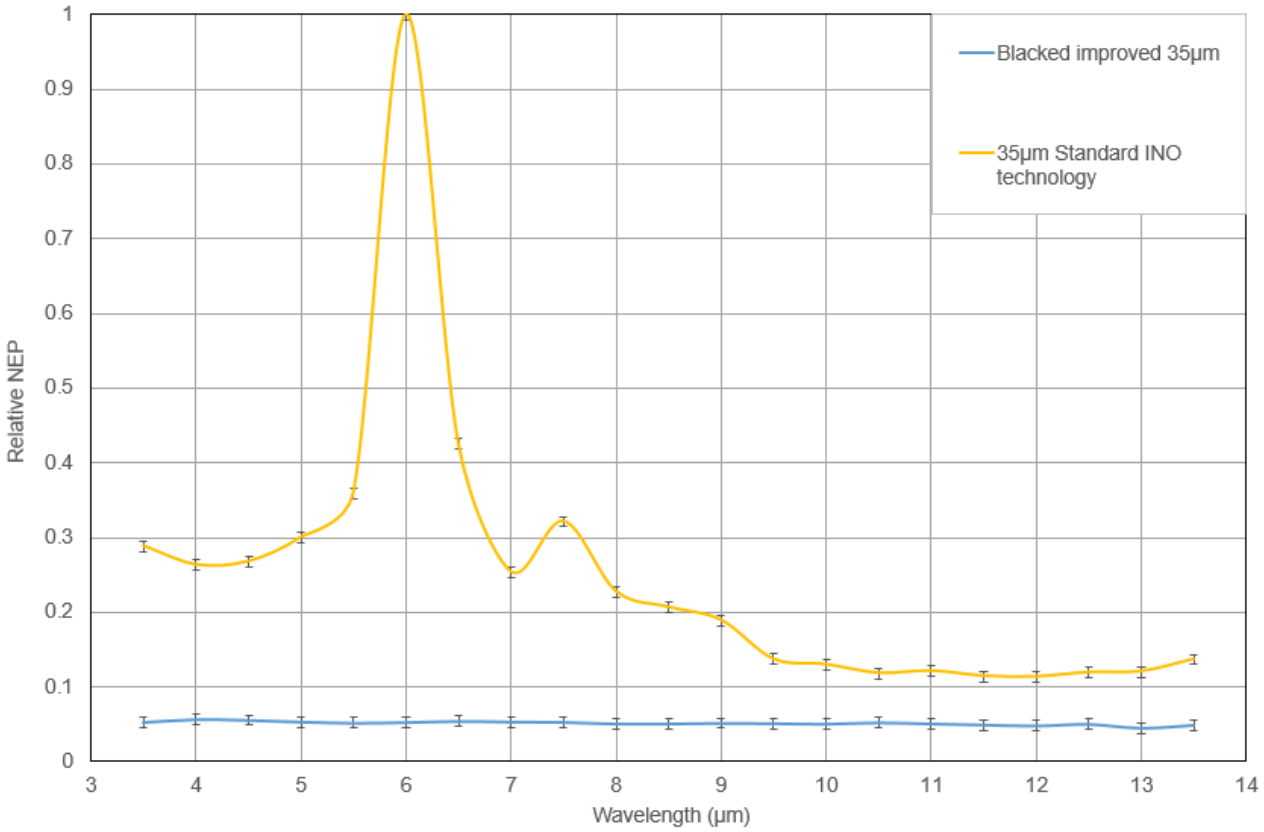

Figure 10. NEP as function of the wavelength for both INO's standard 384 x 288 FPA and updated 384 x 288 FPA with gold black.

4.3 Detectivity results

The spectral responsivity over the wavelength range from 3 to 14µm was measured with a monochromator. The monochromator output was calibrated with two independent reference detectors, namely a pyroelectric detector and an InGaAs detector. The reference detector aperture was overfilled using appropriate optical elements, and the power density was deduced from the nominal detector area. During the measurements, the lamp of the monochromator output was modulated to reduce the contribution from the radiative environment and emission from the optics (lens, grating). The output of the reference detectors was demodulated by a digital lock-in amplifier and logged by a data acquisition software. The spectral resolution of the monochromator source was set to 50 nm.

Following the calibration of the power density, the two packages were mounted on INO's MicroXcam electronics and exposed to the same modulated monochromatic source. The signal within the region of interest was averaged for each frame and demodulated by a software algorithm. The responsivity was computed by dividing the signal by the power spectral density. Figure 11 shows the relative detectivity thus obtained. For wavelengths below 8 µm, the detectivity is more than 5 times higher for the new INO 384 x 288 FPA with gold black. Also, as for the NEP, the detectivity is uniform over the whole spectral band.

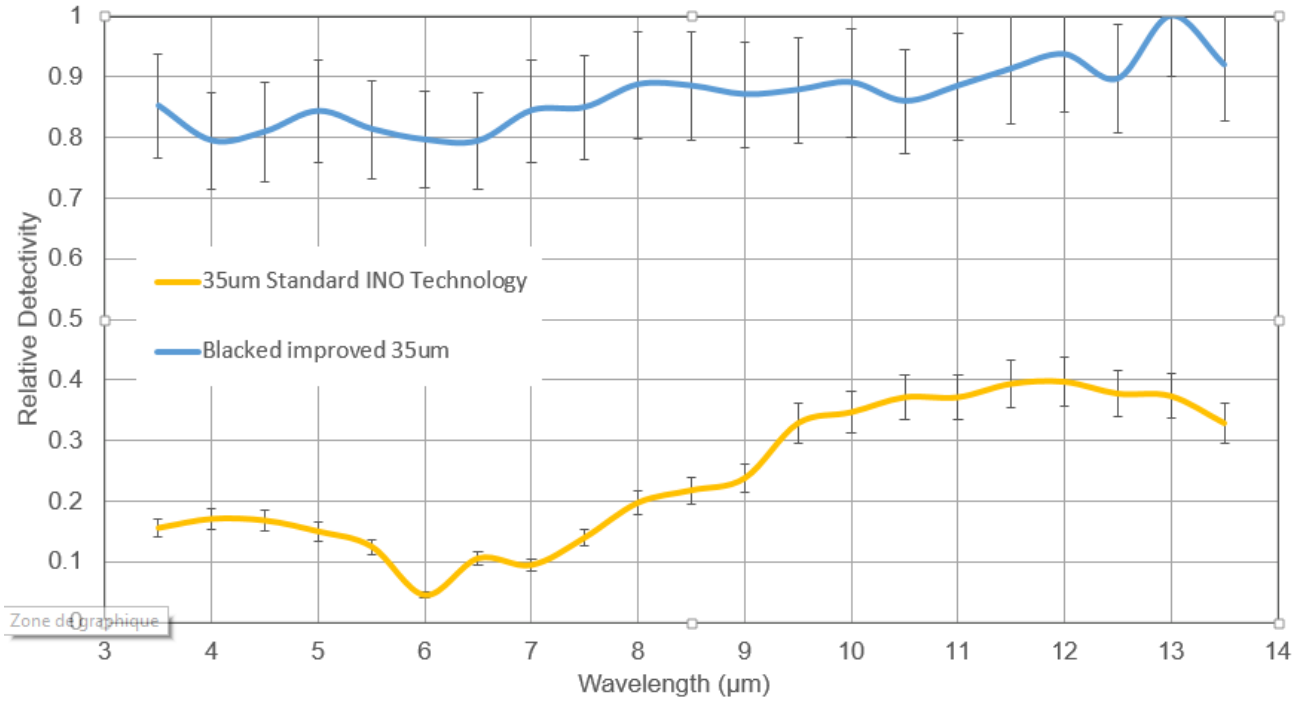

Figure 11. Detectivity of packaged FPAs from 3.5 to 13.5µm.

4.4 Response time results

The methodology used to measure the response time in the packages has been described in a previous paper[19]. The window of the package acts as filter in the current experimental setup.

The measured response time of a standard INO 384 x 288 FPA without gold black was shown to be 11 ms in agreement with the previously reported value[27]. The updated INO 384 x 288 FPA with gold black has a much longer response time at 22 ms. The product of NETD multiplied by τ (where τ is the response time) is lower than the value for other 35 µm pitch bolometers currently produced[28].

4.5 MRTD results

To evaluate the effect of gold black on the minimum resolvable temperature difference (MRTD), we measured the MTF for INO's packaged updated 384 x 288 FPA with gold black and the standard INO 384 x 288 FPA. The MTF was measured with an F-0.86 optics in the 8-12 µm wavelength range. Figure 12 shows the relative MTFs of the two packaged FPAs normalized to INO's standard 384 x 288 FPA at zero spatial frequency. Despite laser trimming of the gold black layer, the MTF is slightly worse for the packaged updated 384 x 288 FPA. Residual gold black coating in the trenches creating thermal shorts is a hypothesis for the slight degradation of the MTF. We are currently working to improve the MTF.

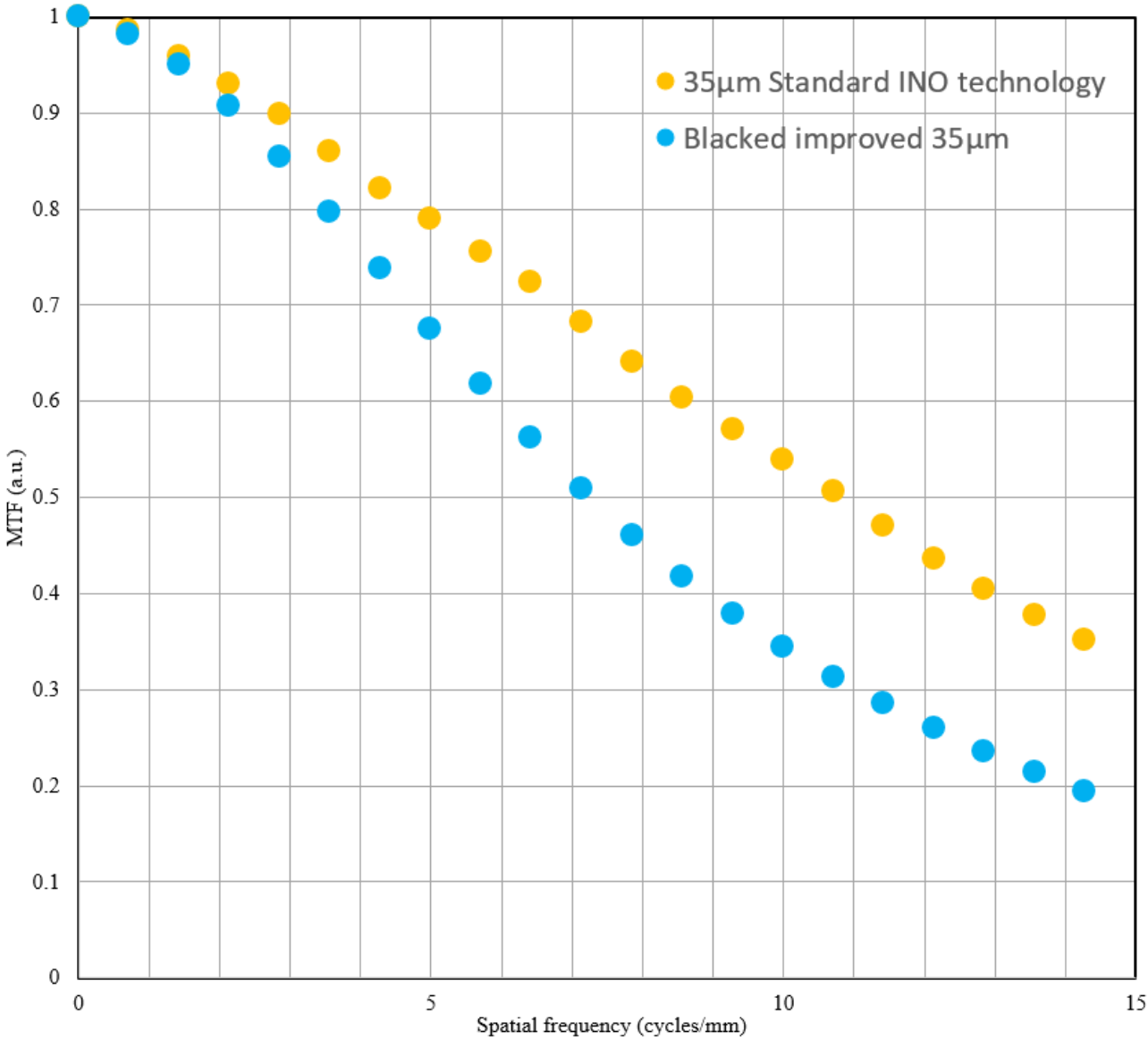

Figure 12. Relative MTF for packaged FPAs from 3 to 14µm with respect to the spatial frequency.

The MRTD was then obtained using the following equation.

MRTD = k*NETD/MTF

where k is a constant that relies on pixel pitch and optics. We defined the figure of merit with regards to spatial frequency (FOM(f)) as:

FOM(f) = MRTD*τ

Figure 13 shows the FOM(f) for the two packaged FPAs. The FOM(f) is 35% lower at f=0 for the updated INO's 384 x 288 FPA with gold black in comparison to our standard FPA without gold black. For high spatial frequencies, the FOM(f) of the two FPAs is similar. In the case of the current FPAs, the Nyquist frequency is 15 cycles/mm.

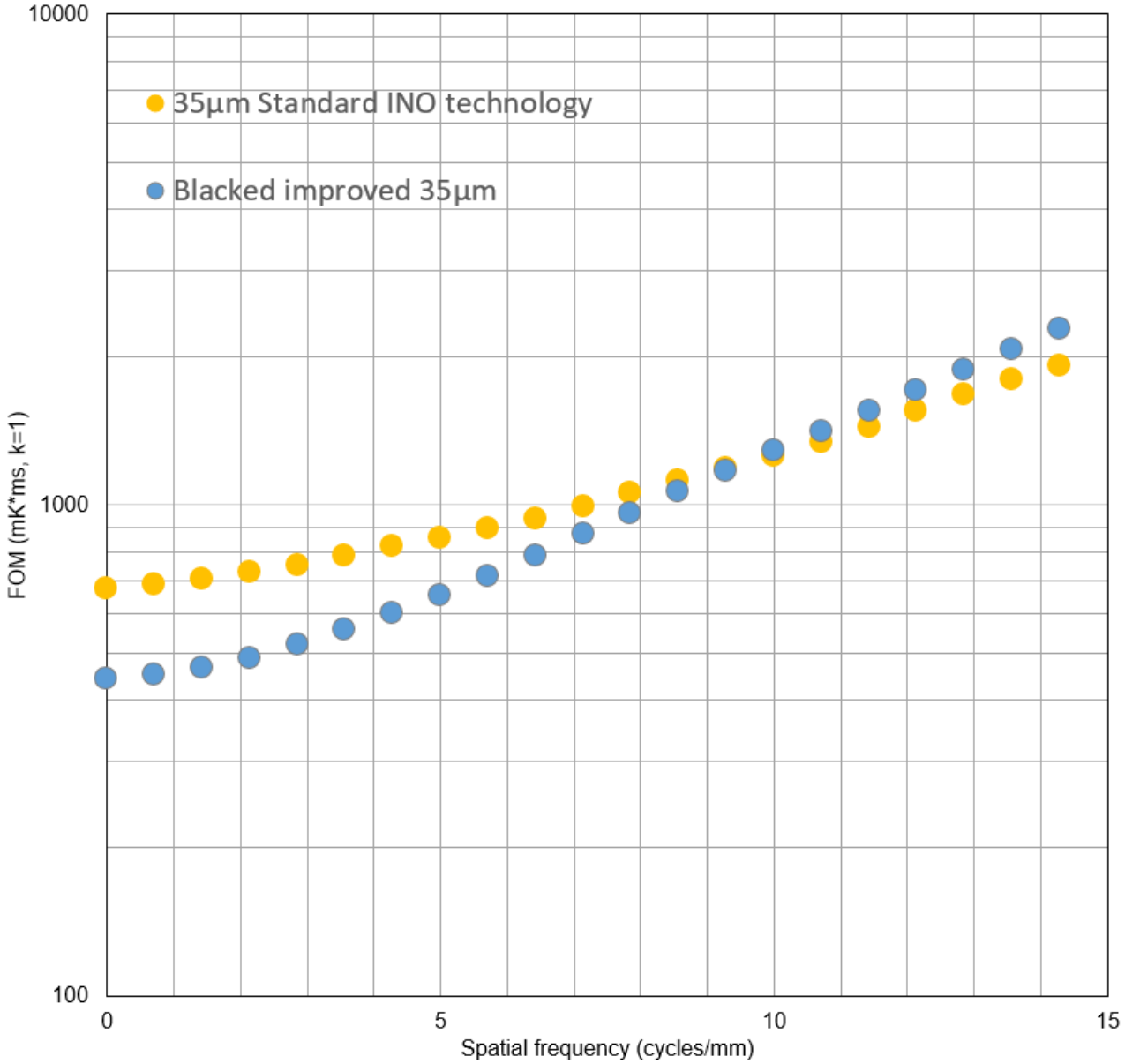

Figure 13. Figure of merit for packaged FPAs from 3 to 14µm with respect to the spatial frequency.

5. CONCLUSIONS

We have designed a package and developed a low temperature packaging process to produce vacuum-sealed microbolometer FPAs with a temperature sensitive gold black coating. The detector makes use of a gold black thin film to improve its absorption range from 3 to 14 µm. The packaging solution allows for a low base pressure and this pressure remains stable with time because of good hermeticity and the very low outgassing. The packaged FPA package developed herein could be applied to other wavelengths bands, thanks to the broadband absorption of gold black thin films.

The performances of the packaged detector were measured in terms of NETD, NEP, detectivity and response time. The resulting FPAs shows a NETD of 22 mK at a frame rate of 50 Hz. The MRTD is also significantly better than INO's standard FPA for spatial frequencies below 10 cycles/mm. Work is currently underway to extend this improvement to higher spatial frequencies.

ACKNOWLEDGEMENTS

The development of the new high speed laser station with micrometric accuracy used for the work presented in this paper has been funded by the Canadian Space Agency.

REFERENCES

[1] Jerominek, H., Pope, T.D., Alain, C., Picard, F., Fuchs, R.W., Lehoux, M., Zhang, R., Grenier, C., Rouleau, Y., Cayer, F., Savard, S., Bilodeau, G., Couillard, J.-F. and Larouche, C., "128x128 pixel uncooled bolometric FPA for IR detection and imaging," Proc. SPIE 3436, 585-592 (1998).

[2] Pope, T., Jerominek, H., Alain, C., Cayer, F., Tremblay, B., Grenier, C., Topart, P., LeClair, S., Picard, F., Larouche, C., Boulanger, B., Martel, A. and Desroches, Y. "Commercial and custom 160x120, 256x1, and 512x3 pixel bolometric FPAs " Proc. SPIE 4721, 64-74 (2002).

[3] Pope, T. D., Jerominek, H., Alain, C., Picard, F., Fuchs, R. W., Lehoux, M., Zhang, R., Grenier, C., Rouleau, Y., Cayer, F., Savard, S., Bilodeau, G., Couillard, J.-F. and Larouche, C., "256x1 and 256x40 pixel bolometer arrays for space and industrial applications," Proc. SPIE 3436, 325-331 (1998).

[4] Ngo Phong, L. and Pope, T. D., "Linear arrays of microbolometers for space applications," Proc. 7th IEEE Sensors Conf., 1344-1347 (2008).

[5] Proulx, C., Williamson, F., Allard, M., Baldenberger, G., Gay, D., Garcia-Blanco, S., Côté, P., Martin, L., Larouche, C., Ilias, S., Pope, T., Caldwell, M., Ward, K. and Delderfield, J., "The EarthCARE broadband radiometer detectors," Proc. SPIE 7453, 74530S1-74530S11 (2009).

[6] Chevalier, C., Mercier, L., Duchesne, F., Gagnon, L., Tremblay, B., Terroux, M., Généreux, F., Paultre, J.-E., Provençal, F., Desroches, Y., Marchese, L., Jerominek, H. Alain, C. and Bergeron, A., "Introducing a 384x288 Pixel Terahertz Camera Core," Proc. SPIE 8624, 8624F1-8624F8 (2013).

[7] Ngo Phong, L., Proulx, C., Oulachgar, H. and Châteauneuf, F. "Far infrared microbolometers for radiometric measurements of ice cloud" Proc. SPIE 9375, 93750G1-93750G11 (2015).

[8] Libois, Q., Proulx, C., Ivanescu, L., Coursol, L., Pelletier, L.S., Bouzid, Y., Barbero, F., Girard, E. and Blanchet, J.P. "A microbolometer-base far infrared radiometer to study thin ice clouds in the Artic" Atmos. Meas. Tech. 9, 1817-1832 (2016).

[9] Proulx, C., Ngo Phong, L., Lamontagne, F., Wang, M., Fisette, B., Martin, L. and Châteauneuf, F. "Development of a far infrared radiometer (FIRR) for sensing of thin ice clouds" Proc. SPIE 9973, 9973-14 (2016).

[10] Garcia-Blanco, Topart, P., Desroches, Y., Caron, J.S., Williamson, F., Alain, C., Pope, T. and Jerominek, H. "Low-temperature vacuum hermetic wafer-level package for uncooled microbolometer FPAs" Proc. SPIE 6884, 68840P1-68840P8 (2008).

[11] Garcia-Blanco, S., Ilias, S., Williamson, F., Généreux, F., Le Noc, L., Poirier, M., Proulx, C., Tremblay, B., Provençal, F., Desroches, Y., Caron, J.S., Larouche, C., Beaupré, P., Fortin, B., Topart, P., Picard, F., Alain, C., Pope, T. and Jerominek, H. "MEMS/MOEMS foundry services at INO" Proc. SPIE 7750, 77500R1-77500R10 (2010).

[12] Topart, P., Picard, F., Ilias, S., Alain, C., Chevalier, C., Fisette, B., Paultre, J.E., Généreux, F., Legros, M., Lepage, J.F., Laverdière, C., Ngo Phong, L, Caron, J.S. and Desroches, Y. "Heteregeneous MEMS device assembly and integration" Proc. SPIE 8975, 89750E1-89750E13 (2014).

[13] Fisette, B., Chevalier, C., Lépine, A., Boucher, M.-A., Larouche, C., Tremblay, M., Lemieux, D., Tremblay, L.-P., Dufour, D., Desroches, Y., Topart, P. and Châteauneuf, F., "Design and fabrication of a scalable high-reliability vacuum sealed package for infrared detectors", 2012 4th Electronic System-Integration Technology Conference 6542149 (2012).

[14] Garcia-Blanco, S., Cote, P., Leclerc, M., Blanchard, N., Desroches, Y., Caron, J.S., Ngo Phong, L., Chateauneuf, F. and Pope, T. "Radiometric packaging of uncooled microbolometer FPA arrays for space applications" Proc. SPIE 7206, 720604-1-720604-12 (2009).
[15] Ilias, S., Topart, P., Larouche, C., Beaupré, P., Gay, D., Proulx, C., Pope T. and Alain, C. "Deposition and characterization of gold black coatings for thermal infrared detectors" Proc. SPIE 7750, 77501J1-77501J10 (2010).
[16] Allard, M., Martin, L., Proulx, C., Bouchard, J.P., Cote, P., Oulachgar, H., Delderfield, J., Parker, D. and Chateauneuf, F. "Current Satus of the EarthCARE BBR Detectors Development" Proc. SPIE 8176, 81761E1-81761E10 (2011).
[17] Ngo Phong, L., Alazzam, A., Daly, M., Proulx, C. and Chateauneuf, F. "Net flux sensor for the measurement of Mars surface radiation budget" Proc. SPIE 8252, 82520A1-82520A12 (2012).
[18] Becker, W., Fettig, R., Gaymann, A. and Ruppel, W., "Black gold deposits as absorbers for far infrared radiation", Phys. Stat. Sol. (B), 194, pp. 241-255 (1996).
[19] Généreux, F., Tremblay, B., Girard, M., Paultre, J.-E., Provençal, F., Desroches, Y., Oulachgar, H., Ilias, S. and Alain, C., "On the figure of merit of uncooled bolometers fabricated at INO" Proc. SPIE 9819, 98191U1-98191U9 (2016).
[20] Mercier, L., Fisette, B., Terroux, M., Desroches, Y., Beaupré, P., Demers, M., Dufour, D., Généreux, F., Marchese, L., Topart, P., Alain, C. and Bergeron, A., " Wideband sensitive THz core for application integration" Proc. IRMMW-THz 2015 - 40th Conference on Infrared, Millimeter and Terahertz waves, 7327591 (2015).
[21] Sisto, M.M., Garcia-Blanco, S., Le Noc, L., Tremblay, B., Desroches, Y., Caron, J.S., Provencal, F. and Picard, F., "Pressure sensing in vacuum hermetic micropackaging for MOEMS-MEMS" Proc. SPIE 7592, 759204-1-759204-10 (2010).
[22] O'Hanlon, J. F., *A User's Guide to Vacuum Technology*, 3rd edition, John Wiley & Sons, 516p (2003).
[23] Nelms, N., Dowson, J., Rizvi, N. and Rohr, T., "Laser micromachining of goldblack coatings" Applied Optics, 45(27), 6977-6981 (2006).
[24] Desbiens, L., Deladurantaye, P., Cournoyer, A., Gay, D., Paré, C., Eiselen, S., Roy, V. and Taillon, Y., "Flexible and Programmable Pulse Shaping MOPA Fiber Laser Platform, Performances and Applications, Rev. Laser Eng., Vol 41, No 9, (2013).
[25] Niklaus, F., Jansson, C., Decharat, A., Kallhammer, J.E., Pettersson, H. and Stemme, G., "Uncooled infrared bolometer arrays operating in a low to medium vacuum atmosphere: Performance model and tradeoffs" Proc. SPIE 6542, 65421M1-65421M12 (2007).
[26] Sisto, M.M., Garcia-Blanco, S., Le Noc, L., Tremblay, B., Desroches, Y., Caron, J.S., Provencal, F. and Picard, F., "Pressure sensing in vacuum hermetic micropackaging for MOEMS-MEMS" J. Micro/Nanolith. MEMS MOEMS, 9(4) 041109 (2010).
[27] INO, ''384x288 FPA Uncooled bolometric detector'', <http://www.ino.ca/media/187150/fiche-matrice-bolométrique-384x288.pdf> (17 February 2017).
[28] Skidmore, G.D., Han, C.J. and Li, C., "Uncooled Microbolometers at DRS and Elsewhere Through 2013" Proc. SPIE 9100, 910003-1-910003-5 (2014).